

Robust Hydroxyapatite Coating by Laser-Induced Hydrothermal Synthesis

Seung-Hoon Um, Yong-Woo Chung, Youngmin Seo, Hyunseon Seo, Myoung-Ryul Ok, Yu-Chan Kim, Hyung-Seop Han, Justin J. Chung, James R. Edwards, and Hojeong Jeon*

Owing to enhanced biocompatibility and osseointegration, hydroxyapatite (HAp) coatings are often applied to biomedical devices that are implanted directly on the bone. Although various HAp coating techniques have been developed, they are restricted due to the time-consuming HAp synthesis and additional coating processes. Herein, the development of a rapid single-step method for simultaneous synthesis and coating of HAp via nanosecond laser surface treatment is described. In the conventional HAp-coating method, the resulting interface between the HAp layer and the base material is clearly distinguished. However, in this method, HAp synthesis and coating occur simultaneously via the melting of the base material (i.e., titanium, polyetheretherketone, and polycaprolactone) to form a gradient HAp-base material composite coating layer. The resultant coating layer on a titanium surface exhibits a binding force of 31.7–47.2 N, which is sufficient for medical implant applications. Changing the laser irradiation conditions provides quantitative adjustment of the HAp formation process and coating layer thickness. Furthermore, the resulting HAp coating layer better facilitates the attachment of bone cells. These results offer a breakthrough in the surface treatment of bone-bonding sites of metal and polymer biomedical devices.

1. Introduction

Titanium-based bone fixation devices are commonly used to treat broken bones in the human body^[1–3] due to its excellent mechanical properties and biocompatibility.^[4,5] To further enhance the osteoconductive properties, titanium is normally coated with hydroxyapatite (HAp), which is an inorganic component of bones.^[6–9] HAp-coated materials tend to show better biocompatibility, bone-forming ability, and osteoconductivity when compared to materials without a HAp coating.^[10–13] Various HAp coating methods, such as sol–gel coating,^[14–16] dip coating,^[17,18] electrochemical deposition,^[19,20] electrophoretic deposition,^[21,22] plasma spraying,^[23,24] sputter coating,^[25,26] hot isostatic pressing,^[27–29] and biomimetic coating,^[30,31] have been developed in the past. However, most of the existing methods require a separate synthesis process for HAp coating.^[32,33] Sol–gel, dip, and biomimetic coating methods do not require the preliminary synthesis


process, but they require time-consuming reactions that last for several days,^[14,17,30] and are difficult to use in clinical practice due to their poor coating adhesion strength.^[33–35] Attempts have been made to create HAp coatings using lasers such as pulsed laser deposition; however, they required a separate HAp synthesis either using a HAp plate as a target^[36–39] or by laser soldering of sprayed HAp powder on the surface.^[40,41] The pulsed lasers may also provide a heat source in the hydrothermal process, which is widely used in nanowire^[42] and nanorod^[43] synthesis processes. A few studies have tried to synthesize and form HAp nuclei using laser-based hydrothermal process; however, these processes were not applicable for medical implants due to the poor binding strength of the coating layer.^[44–46] In this study, we introduced a method of simultaneous synthesis and coating of HAp in a single process to form a HAp–substrate mixed molten layer in which HAp penetrates into the substrate. This coating method involves irradiating laser pulses onto an immersed metallic or polymeric specimen in a precursor solution containing calcium and phosphoric acid, the synthesis of HAp from the solution containing calcium and phosphate ions, and the formation of the coating layer due to surface melting occurred simultaneously on the laser-treated surface. By controlling the laser irradiation conditions, different amount and thickness of the HAp coating

S.-H. Um, Y.-W. Chung, Dr. Y. Seo, H. Seo, Dr. M.-R. Ok, Dr. Y.-C. Kim, Dr. H.-S. Han, Dr. J. J. Chung, Dr. H. Jeon
Center for Biomaterials
Biomedical Research Institute
Korea Institute of Science and Technology (KIST)
Seoul 02792, Republic of Korea
E-mail: jeonhj@kist.re.kr

S.-H. Um
Dental Research Institute and Department of Biomaterials Science
Seoul National University
Daehakro 101, Jongno-gu, Seoul 03080, Republic of Korea

Dr. Y.-C. Kim, Dr. H. Jeon
Division of Bio-Medical Science and Technology
KIST School
Korea University of Science and Technology
Seoul 02792, Republic of Korea

Prof. J. R. Edwards
Botnar Research Centre
Nuffield Department of Orthopaedics
Rheumatology and Musculoskeletal Sciences (NDORMS)
University of Oxford
Oxford OX3 7LD, UK

 The ORCID identification number(s) for the author(s) of this article can be found under <https://doi.org/10.1002/adfm.202005233>.

DOI: 10.1002/adfm.202005233

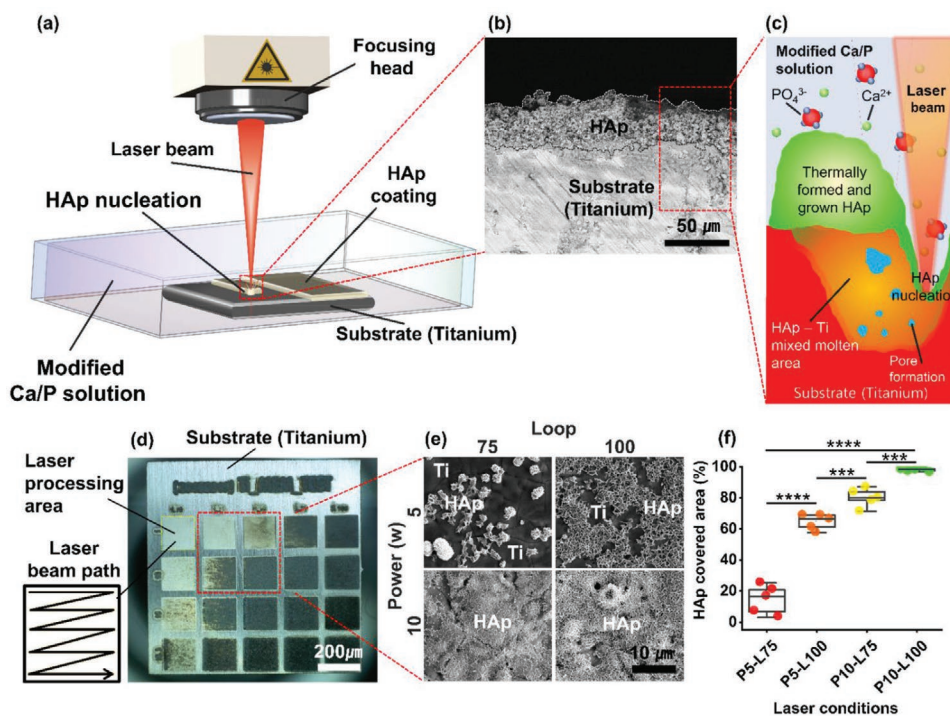


Figure 1. a) Schematic diagram of the hydroxyapatite coating layer formed by the laser-induced single-step coating (LISSC) process on titanium surface with modified apatite coating solution (MACS) and nanosecond laser. b) SEM image of the cross-section of hydroxyapatite (HAp)-coated surface. c) Schematic diagram of the hydroxyapatite nucleus and coating layer formation by laser radiation in MACS solution. d) The optical image of the specimen surface-treated under various laser conditions and the “laser beam path” used in laser processing. e) SEM images of the coating layer with a controlled amount of hydroxyapatite formation under laser emission conditions. f) Comparison of HAp formation area (%) according to laser emission conditions. “P” and “L” indicate power and loop, respectively. Data represent mean \pm s.d., ***, **** indicate statistically significant difference when value compared to each comparison group with *** p < 0.001, **** p < 0.0001.

was observed. More importantly, the HAp layer formed by the laser-induced single-step coating (LISSC) process exhibits a high coating strength that is sufficient for medical use.^[47,48]

2. Results and Discussion

2.1. HAp Synthesis and Coating in a Single-Step Process Using the Nanosecond Laser

HAp synthesis and coating were realized in a single-step process by immersing a titanium alloy (Ti–6Al–4V) in a modified apatite coating solution (MACS) containing calcium and phosphoric acid (Table S1, Supporting Information) and then irradiating nanosecond laser pulses on the titanium surface (Figure 1a–c, and Movie S1, Supporting Information). When the laser power density was varied in the range of 0.1–3539 W mm^{−2}, we observed that the surface melting started at 100 W mm^{−2} or more (Figure S1, Supporting Information). The synthesized HAp was observed when the laser power density was higher than 1770 W mm^{−2}, with the number of loops (L) as 75 or higher (Figure 1d–e). The amount of HAp formed on the surface was controlled by the power and L of the laser using this tendency. We compared the synthesized HAp layers formed by LISSC with laser powers (P) of 5 and 10 W and L of 75 and 100. The HAp covering areas at different P and L combinations were $14.5 \pm 9.4\%$ (P5-L75), $64.6 \pm 5.1\%$ (P5-L100), $80.2 \pm 6.0\%$ (P10-L100), and $98.2 \pm 1.1\%$ (P10-L100) (Figure 1f and

Figure S2, Supporting Information). At $P = 10$ W, the HAp layer was generated even when L was 50 (Figure 2). Thin-film X-ray diffraction (XRD) pattern analysis showed that the coating layer matched well with Ca₁₀(PO₄)₆(OH)₂, which is the HAp phase^[49] (JCPDS 09–0432). Additionally, the coating layer was scraped off and analyzed in a powdered state, which also showed the HAp phase (Figure 2a and Figure S3, Supporting Information). For both P10-L50 and P10-L100, the calcium–phosphate ratio was approximately 1.64 ± 0.04 and 1.65 ± 0.07 in energy-dispersive X-ray (EDX) analysis, and 1.6732 ± 0.0055 and 1.6663 ± 0.0063 in inductively coupled plasma optical emission spectroscopic (ICP-OES) analysis, respectively. The ratio obtained from the ICP-OES analysis is similar to the calcium–phosphate ratio of the known HAp (1.67)^[50] (Figure 2b–d and Figure S2, Supporting Information). To analyze HAp without affecting the base material, the phase analysis was performed by scraping HAp off the surfaces of P10-L50 and P10-L100. As a result, a pure HAp phase without a titanium peak and a relatively high crystallinity were observed (Figure 2a and Figure S3, Supporting Information). Interestingly, the crystallinity of HAp increased as the number of loops increased (Figure S4, Supporting Information). The results showed that the crystallinity can be controlled by the laser processing conditions, particularly L . In addition, this method allows not only the formation of the coating layer, but also the graphic implementation by a laser direct ablation process with different immersion solutions (Figure S5, Supporting Information). The HAp patterns implemented by this method are of various shapes, such as lines, curves, and text.

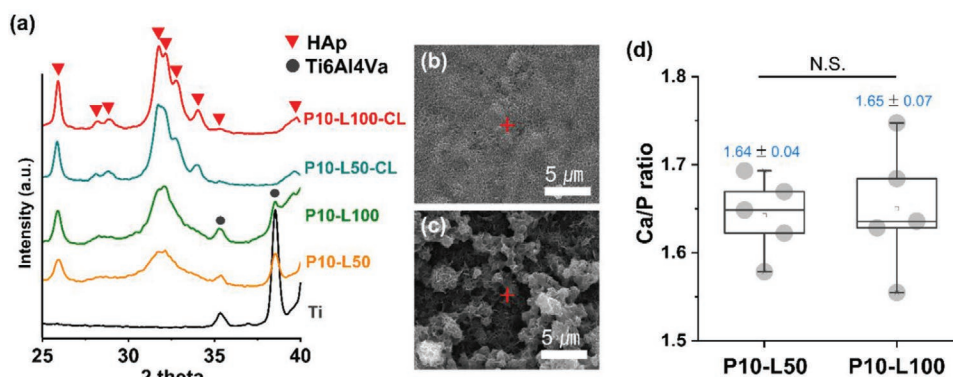


Figure 2. a) Phase analysis of the surface coating layer using thin-film mode in XRD (P10-L50, P10-L100), and scraped off the surface coating layer (P10-L50-CL, P10-L100-CL). SEM images of P10-L50 condition (b) and P10-L100 condition (c) surfaces which performed EDS (energy dispersive spectrometry) elemental analysis. d) The calcium and phosphate ratios obtained from EDS elemental analysis. Data represent mean ± s.d.; N.S. indicates that the comparison of each group is not significant.

2.2. Analysis of the Thickness and the Strength of the Surface Coating Layer

Cross-sectional elemental mapping analysis was performed to determine the thickness and the composition of the surface

coating layer. The mapping of the calcium and phosphate elements, which are the major compositional elements of HAp,^[51] indicated that the thickness of the HAp coating layers were $20.3 \pm 4.6 \mu\text{m}$ and $53.3 \pm 11.5 \mu\text{m}$ for P10-L50 and P10-L100 laser conditions, respectively (Figure 3a–d).

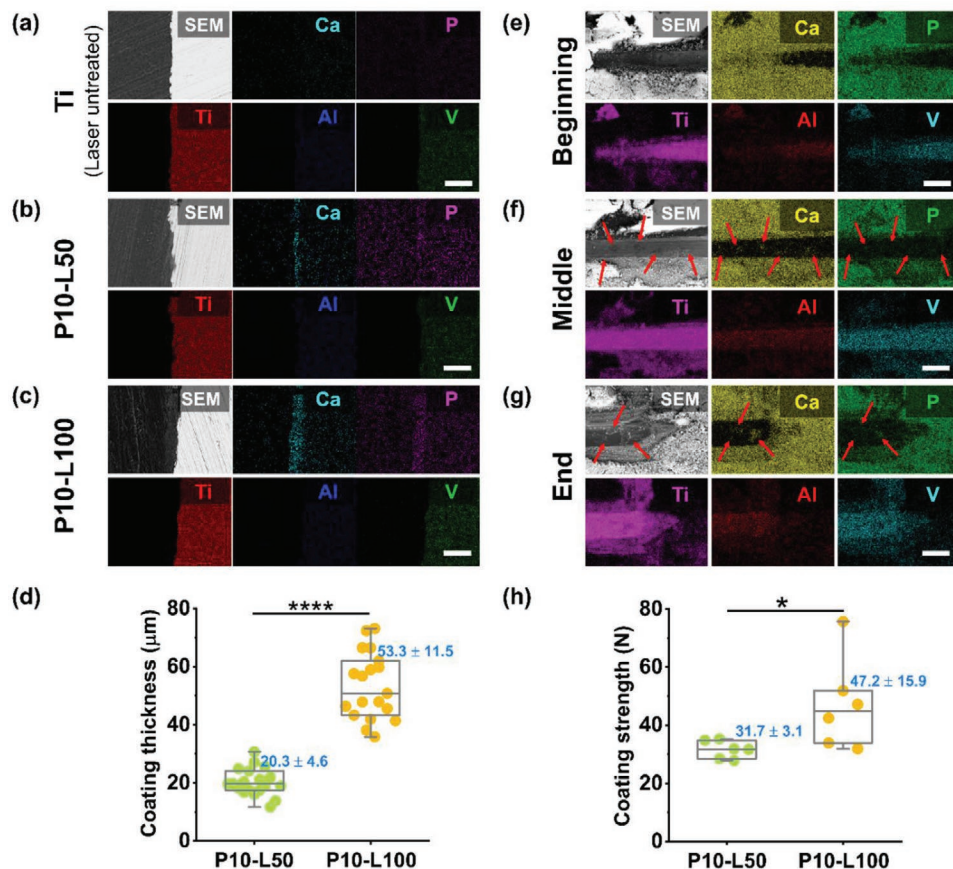


Figure 3. Cross-sectional SEM (top left) and EDX mapping images of HAp coating layer by laser irradiation condition: a) Ti, b) P10-L50, c) P10-L100 (scale bar 100 μm). HAp coating thickness (d) with laser radiation conditions. Images of SEM (top left) and EDX analysis of surface element after the scratch test at the beginning (e), middle (f), and end (g) area of the scratch. The red arrow indicates HAp that remains on the surface after the scratch test (scale bar 100 μm). HAp coating strength (h) with laser radiation conditions. Data represent mean ± s.d. *, **** indicate statistically significant difference when value compared to each comparison group with * $p < 0.05$, **** $p < 0.0001$.

In addition, during the laser-induced surface treatment, the titanium surface melted repeatedly, forming micropores,^[52,53] thus resulting in a valley-like rough surface.^[54,55] In the LISSC method, HAp synthesis and coating were carried out simultaneously during the formation of the valley-like surface (Figure S6, Supporting Information). Therefore, HAp was not only adsorbed on the surface of the melting layer but also formed deep in the valley-like structure (Figure S7, Supporting Information). Because of the combined layers of the structures and the coatings, HAp could remain firmly on the material surface even under harsh conditions such as sanding off the HAp layer (Figure S8, Supporting Information). The improvement in the durability of the HAp coating due to the complex structural properties was also observed in the scratch test (Figure 3e–g). The coating strengths measured by the scratch test were 31.7 ± 3.1 N and 47.2 ± 15.9 N for P10-L50 and P10-L100 laser conditions, respectively (Figure 3h). It was reported that the coating strengths of the layers formed by the dip coating, pulsed laser deposition, and the plasma-spray methods used in medical implant surface treatment^[56,57] were $0.002\text{--}2$ N,^[58,59] $0.6\text{--}5.29$ N,^[60,61] and 11.18 N,^[62] respectively, whereas, the coating method developed in this study provided a comparatively higher coating strength ($31.7\text{--}47.2$ N), which is sufficient for use in clinical practice (Table S3, Supporting Information).

To confirm why the LISSC method provided a high adhesion strength of the coating layer, we carried out structural and elemental analysis using transmission electron microscopy (TEM) (Figure 4a). The coating layer consisted of three layers: 1) HAp, which mainly consisted of calcium and phosphorus, was located on the upper side; 2) titanium was located on the lower side (Figure 4b); and 3) an intermediate layer that was observed at the HAp–titanium interface, in which

HAp and titanium components were mixed and appeared simultaneously (Figure 4c–e and Figure S9, Supporting Information). It can be noted that the intermediate layer improves the coating strength.

2.3. Principle of Single-Step HAp Synthesis and Coating through Laser Irradiation

To further understand the principle of HAp synthesis through laser irradiation, the position of the laser focal point was fixed, and the formation of HAp was observed (Figures 5 and 6 and Figure S10, Supporting Information). When a titanium specimen was immersed in distilled water and then irradiated with laser pulses, only ablated craters and heat-affected areas were observed, and no calcium or phosphate components were detected (Figures 5a and 6a and Figure S10a, Supporting Information). When a titanium specimen was immersed in Dulbecco's modified eagle medium (DMEM) containing inorganic ions similar to body fluid, calcium and phosphate components were formed around the ablated spot (Figures 5b and 6b and Figure S10b, Supporting Information). When a titanium specimen was immersed in MACS containing inorganic ions similar to body fluid and the concentration of calcium and phosphate was increased 100 times, HAp-covered circles were formed around the ablated spot (Figures 5c and 6c, and Figure S10c, Supporting Information). This result indicates that HAp synthesis occurs when the laser is radiated to a precursor solution containing calcium and phosphate ions. The amount of HAp formation increases when the thermal energy applied to the sample increases through increases of P and L (Figure S2, Supporting Information). This behavior is similar to the conventional hydrothermal synthesis method where the thermal

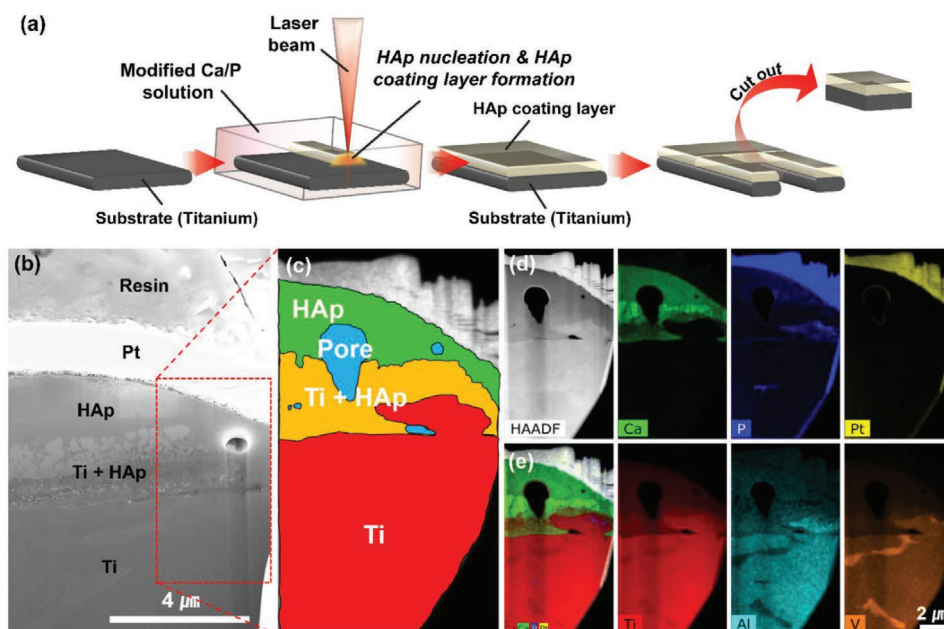


Figure 4. a) Schematic diagram of the sample preparation process for analyzing the structure of the coating layer. b) BSE image of HAp coating layer cross-section (red dotted line—TEM analysis area). c) Schematic diagram of the element mapping results. d) Cross-section electron microscopy images and elemental mapping analysis using TEM-HAADF. e) Merged element mapping result.

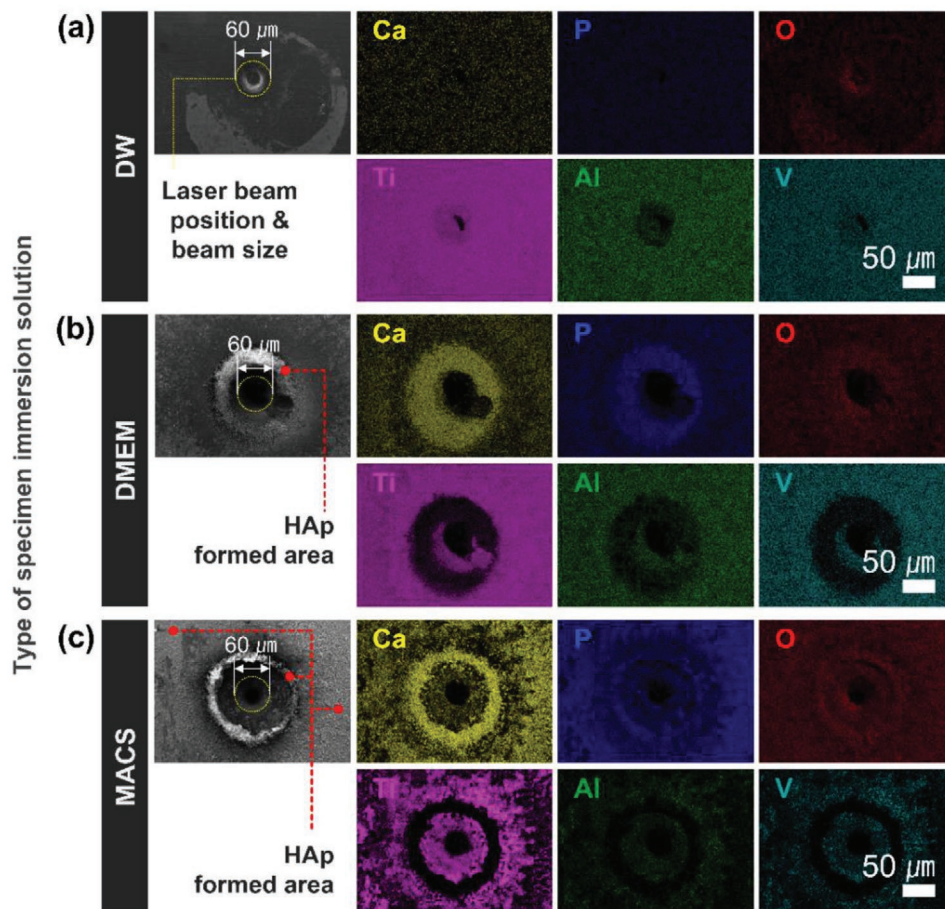


Figure 5. Surface elemental mapping images using SEM, EDX after single-point laser irradiation by immersion solution type. Surface elemental mapping images of titanium immersed in distilled water (a), DMEM (b), and MACS (c) with fixed single-point laser irradiation.

energy applied to the solution is proportional to the amount of synthesized HAp.^[63] Moreover, it has been reported that HAp is formed when a specimen is immersed in a solution containing inorganic ions found in body fluid, such as Hanks' balanced salt solution, DMEM, and simulated body fluid.^[64,65] The reaction governing the HAp synthesis in a solution containing calcium and phosphate ions has been actively studied.^[66–68] These dip coating methods, which do not use a laser process, require 1–15 days to form a 2–10 μm thick HAp coating.^[69,70] To promote the formation of HAp, a method for increasing the concentration of inorganic ions was used.^[71] However, when the concentration of inorganic ions, compared to body fluid, was increased by ten times, it took 2–6 h to form HAp.^[72] In contrast, the 20–30 μm thick HAp coating layer could be formed within 15 min by the LISSC method. From the above results, it is presumed that our method accelerated the rate and amount of HAp nucleation by the multiple effects of the “laser-induced thermal energy” and “high concentration inorganic ions.”

Summarizing the results of the surface, cross-section, microstructure, and elemental analysis, the HAp formation by the LISSC process can be described as follows: The substrate comes in contact with supersaturated calcium and phosphate ions in the MACS solution. The laser is irradiated on the surface of the substrate to increase the temperature locally. The local

melting of the substrate surface due to increased temperature and the HAp nucleation from calcium and phosphate ions due to thermal energy occur simultaneously. The surface melting and the formation of HAp are repeated by multiple loops of laser scanning, whereby HAp penetrates into the substrate to form a HAp–substrate coexisting intermediate layer. The thermal energy formed at the focused spot of the laser beam is transmitted by conduction in the substrate and convection of the solution. As a result, the crystal size of the previously nucleated HAp grows, thus generating a thermally formed-HAp crystal. As the laser beam moves, the substrate heating and melting, HAp nucleation, HAp–substrate intermediate layer formation, and HAp crystal growth phenomena continuously occur to form a coating layer along the path of the laser beam, thereby providing a thick and strong HAp coating layer (Figure 7). Furthermore, when LISSC was applied to polymeric substrates, such as polyetheretherketone (PEEK) and polycaprolactone (PCL), with the laser condition of $P = 10$ W power and $L = 50$, HAp coatings—with the thicknesses of 26.3 ± 6.7 μm and 25.4 ± 4.6 μm , respectively—were well-formed on the surfaces of the substrates (Figures S11–S13, Supporting Information). In the elemental component analysis, calcium and phosphate were detected not only on the surface of the specimen but also inside the base material. (Figures S14 and S15,

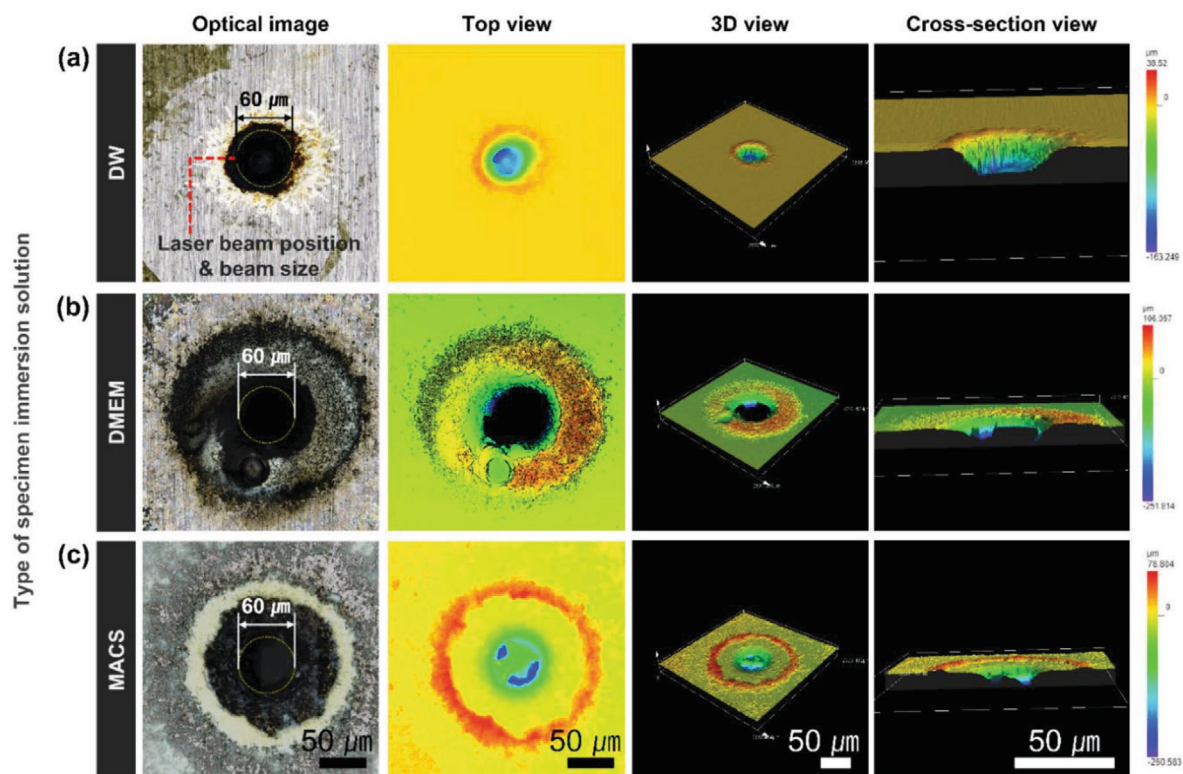


Figure 6. Optical and 3D images after single-point laser irradiation processing by immersion solution type. Surface optical and 3D images of titanium immersed in distilled water (a), DMEM (b), and MACS (c) with fixed single-point laser irradiation.

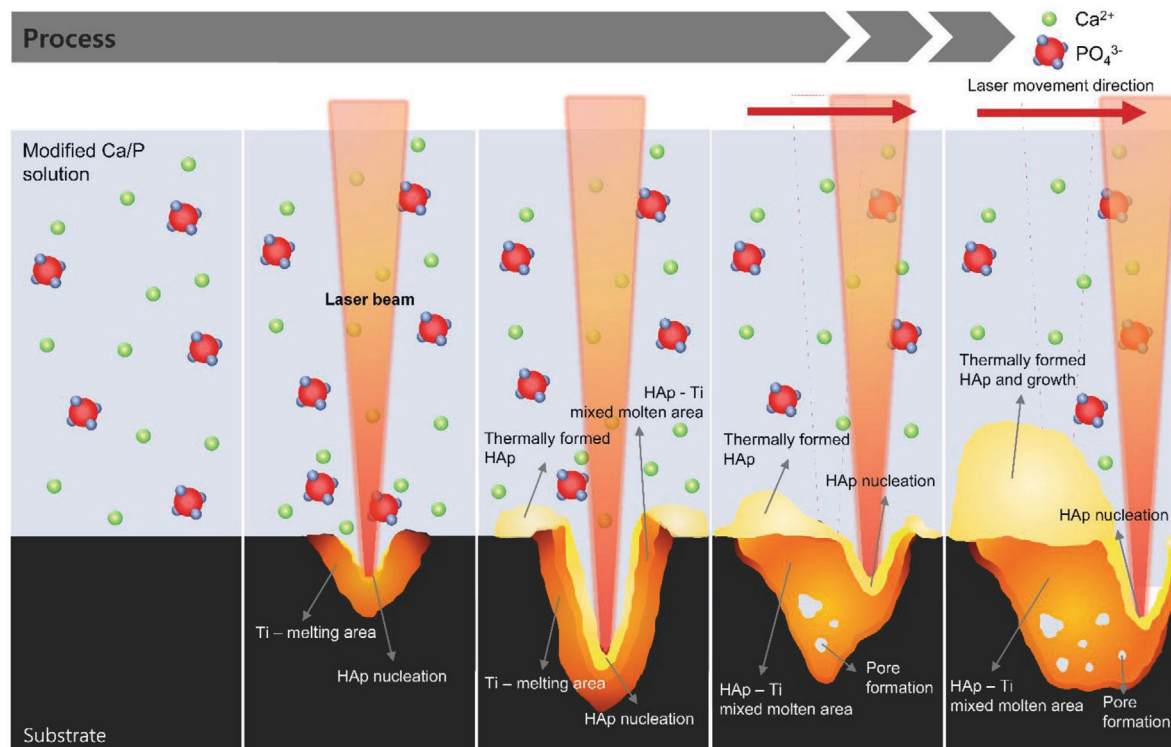


Figure 7. Schematic diagram of the laser-induced single-step coating induced hydroxyapatite synthesis, HAp-substrate mixed molten layer, and HAp coating layer formation process. In the figure, the green and red circles indicate “Ca²⁺”, and “PO₄³⁻” ion, respectively.

Supporting Information). As a result, the LISSC technique, which forms a secure coating layer due to the HAp formation and its penetration in the base material, can be implemented not only in metals but also in polymers.

2.4. Evaluation of the Adhesion of a Bone Cell and Serum Protein on the HAp-Coated Surface Formed by the LISSC Method

We evaluated the adhesion of serum proteins and bone cells (osteoblasts) to confirm the biomedical applicability of the HAp-coated surface formed by the LISSC method. The number of attached cells was considered as a parameter for the assessment of the bone formation potential of a material.^[34,73] Furthermore, it was found that the increase in the number of bone cells on the HAp-coated surface was statistically significant as compared to the number of bone cells on untreated titanium specimens (Figure 8a–c). Serum proteins are known as

essential factors for biocompatibility and bone formation.^[74–76] The serum proteins, particularly fibronectin and vitronectin, are known to promote bone cell adhesion, proliferation, differentiation, and bone formation.^[77–80] In all our results, it was observed that the amount of adsorption of the serum proteins was higher on the specimens processed under the P10-L50 and P10-L100 laser conditions as compared to that on the titanium specimens. Moreover, we found that the thicker the HAp, the stronger the adhesion (Figure 8d and Figure S16, Supporting Information). The surface roughness and hydrophilicity of the specimens treated under P10-L50 and P10-L100 laser conditions increased as compared to the titanium specimens (Figures S17 and S18, Supporting Information). It is assumed that the increase in the number of loops during the laser irradiation thickens the HAp coating layer, thereby increasing the surface roughness and hydrophilicity. Furthermore, it promotes the adhesion of proteins that are beneficial to cell adhesion and growth. We also cultured osteoblast cells on the graphically

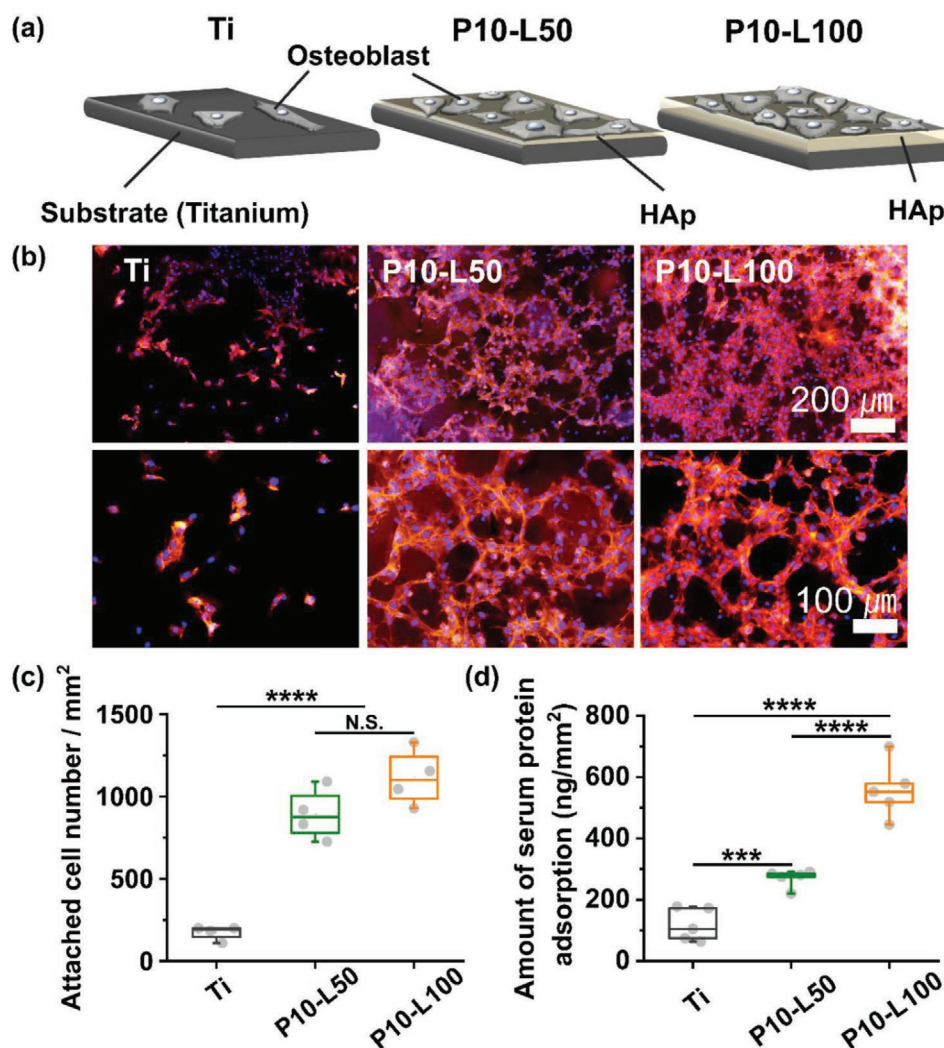


Figure 8. a) The schematic diagram for evaluating the cell adhesion on each surface. b) Fluorescence microscopy images of osteoblasts attached to Ti, P10-L50, and P10-L100 surfaces; nucleus (blue), F-actin (orange). c) The number of osteoblasts attached to the unit area. d) The amount of serum protein adsorbed in the unit area. Data represent mean \pm s.d., ***, **** indicate statistically significant difference when value compared to each comparison group with *** p < 0.001, **** p < 0.0001.

patterned HAp surfaces for 24 h to confirm the effect of the coated HAp. They showed preferential adhesion on the HAp-coated area over the ablated area (Figures S5, S19, and S20, Supporting Information).

3. Conclusions

Herein, we developed a seamless method for synthesizing and coating HAp by using nanosecond laser surface treatment. The technique developed in this study shortened the existing multiple-step process to a single process, thus reducing the total process time from several days to a few minutes. By melting the substrate at the same time as HAp nucleation by laser irradiation, a gradient HAp–substrate intermediate layer in which HAp penetrates into the substrate was observed. The coating thickness could be controlled from $20.3 \pm 4.6 \mu\text{m}$ to $53.3 \pm 11.5 \mu\text{m}$, and it achieved a coating strength of 31.7–47.2 N, which is sufficient for application in medical implants. On the surface treated by the LISSC method, serum proteins and osteoblast adhesion were promoted, thus showing the possibility of application on the surfaces of other biomaterials. Moreover, this coating method could be directly applied to dental and orthopedic implants, and extended to the rough surface of titanium implants that are manufactured by advanced methods such as 3D printing. The LISSC method could also be potentially used for obtaining surface coatings of various compositions by adjusting the elements of the solution used for immersion.

4. Experimental Section

Sample Preparation: Grade 5 titanium (Ti-6Al-4V, 3 mm thick, 10 mm wide, and 10 mm long) specimens were used. The specimens were polished in order of # 300, # 600, and # 1000 using a surface grinder (M-PREP 5, ALLIED), and then washed sequentially in acetone (99.5%, DUKSAN), 99.9% EtOH (DUKSAN), 70% EtOH (DUKSAN), and deionized water (Pure power I, 18.2 M Ω). The washed specimen was used after drying for more than 12 h in a desiccator. PEEK was purchased (Evonik) and machined (U&I) in plate form (2 mm thick, 8 mm wide, and 8 mm long) for use. To remove debris formed during machining, PEEK specimens were washed sequentially in 99.9% EtOH (DUKSAN), 70% EtOH (DUKSAN), and deionized water (Pure power I, 18.2 M Ω). The washed specimen was used after drying for more than 12 h in a desiccator. Sheet-type (1 mm thick, 20 mm wide, and 5 mm long) PCL was prepared using the following method: Priority, PCL was synthesized using ring-opening polymerization technique. ϵ -Caprolactone (99%) was obtained from Alfa Aesar. Chloroform ($\geq 99.5\%$) was obtained from Daejung Chemicals. Methyl alcohol ($\geq 99.8\%$) was obtained from DUKSAN Pure Chemicals. 1-Dodecanol and tin (II) 2-ethylhexanoate were prepared and stored in dry toluene with 0.2 M concentration prior to use. 1-Dodecanol ($\geq 98\%$, Sigma Aldrich) was used as an initiator and tin (II) 2-ethylhexanoate (92.5–100.0%, Sigma Aldrich) was used as a catalyst with the molar ratio of monomer (10 000): initiator (1): catalyst (1). The reagents and magnetic stirrer were introduced in a 100 mL glass ampoule and sealed under vacuum after purging three times with argon. The sealed ampoule was subsequently heated to 150 °C in an oil bath for 24 h with stirring speed of 200 rpm. After the polymerization, the product was dissolved in chloroform. PCL was precipitated in methanol to remove unreacted contents, and dried under vacuum. The PCL dried in sheet form was cut into 20 mm wide and 5 mm long sizes for the experiment.

Preparation of Modified HAp Coating Solution: For the preparation of MACS, DMEM (LM001-05, WELGENE), which is similar in concentration and inorganic ion composition to body fluid and also acts as a buffer, was used as a basic solution. Subsequently, in order to increase the concentration of calcium and phosphorus components 100 times compared to body fluids, 1 M $\text{Ca}(\text{NO}_3)_2$ (C4955, Sigma-Aldrich) and 1 M H_3PO_4 (P5811, Sigma-Aldrich) solutions were used. The final Ca^{2+} ion concentration was 250 mM, and HPO_4^{2-} ion concentration was 100 mM. In order to minimize the formation of precipitates due to ion supersaturation, ion salt solutions were prepared immediately prior to use. In the LISSC process, the temperature of the solution was 25 °C and pH 7.4. The composition and concentration of inorganic components used in solution preparation are presented in Table S1, Supporting Information.

Laser Direct Writing Process: A nanosecond ytterbium fiber laser (Biolino MOPA, Laservall), which provides a peak power of 20 W, pulse duration of 4–200 ns, repetition rates of 1.6–1000 kHz, and spot size 50 μm was used in this study. For rapid HAp coating on titanium, power was fixed to 10 W, pulse duration with 200 ns, repetition rate at 500 kHz, and scan speed of 0.5 m s⁻¹. Power was measured using a low power thermal sensor connected to a power meter (Nova II, Ophir). Before the laser irradiated onto the specimen, the laser power meter was placed directly on the specimen to measure the power and the power meter removed during the laser treatment. The laser beam was moved in a zigzag manner, and the treatment area per laser condition was 1 × 1 mm (Figure 1d). The interval gap of each line was fixed to 10 μm interval of the laser beam. The laser irradiation completed specimen was immersed in distilled water for 10 min and washed repeatedly three times. The washed specimens were stored in the desiccator until further analysis and experiment. For texturing and graphic implementation on HAp by laser direct writing, HAp-coated specimens were prepared by LISSC method. After the specimen was immersed in distilled water, the laser beam was emitted under the condition of power of 10 W, pulse duration with 200 ns, repetition rate at 500 kHz, and a scan speed of 0.5 m s⁻¹, loop 10 for texturing and graphic implementation on HAp. All coating processes were carried out at 25 °C.

Microstructure and Elemental Analysis of HAp Formed by LISSC Method: The microstructure of HAp formed by the LISSC method was confirmed using a field-emission scanning electron microscope (FE-SEM; Inspect F50, FEI). For surface analysis, the LISSC-treated specimen was washed three times with distilled water to remove unreacted salt on the surface and dried in a desiccator for 12 h. Specimens were kept in desiccator until observation. Elemental analysis used EDX spectroscopy (Inspect F50, FEI). The surface morphology was measured with a 3D laser measuring microscope (OLS5000, Olympus). The HAp coating layer formed by the LISSC method was scraped using a surgical knife (ALN, AN02-002-04) to obtain a powdery sample. This sample was immersed in a 3 mol L⁻¹ HCl solution, and ultrasonication was performed for at least 10 min to make a solution. A quantitative and qualitative analysis was subsequently performed using inductively coupled plasma optical emission spectroscopy (ICP-OES; iCAP 6500 Duo, Thermo). Qualitative analysis was performed by selecting Ca, P, Mg, Na, K, an ionic component of the MACS precursor solution used during LISSC process, and Ti used as a substrate. The results of the analysis are obtained by weight (wt)%, converted to atomic (at)%, and calculated by Ca/P ratio. All values are expressed as mean \pm standard deviation, and values below the detection limit of the equipment are indicated as “Not detected”.

Phase Analysis: Phase analysis of the surface coating layer was used TF-XRD (Dmax2500, RIGAKU). The incident X-ray angle was fixed at 1.5° and the XRD patterns were obtained in the (2 θ) diffraction angle range 10° to 45°. The individual HAp crystals were scraped from titanium surface, and XRD patterns were obtained in the (2 θ) diffraction angle range 10° to 80° using Cu K α radiation (40 kV, $\lambda = 1.54051 \text{ \AA}$) with a step size of 0.05°, time per step of 0.2 s. The base material titanium was Ti-6Al-4V (JCPDS no. 04-002-8708), and the surface coated layer was hydroxyapatite (JCPDS file No. 09-0432) in the phase analysis.

Coating Strength Analysis: The coating strength was measured using scratch test equipment (RST3, Anton paar). Scratch measurement conditions consisted of: speed of 6 mm min⁻¹, length of 3 mm,

begin load of 1000 mN, acquisition rate of 30 Hz, and loading rate of 5000 mN s⁻¹. By comparing the results obtained from the scratch test with the SEM and EDX analysis of the stripped parts, the exact location of the stripped parts was determined to obtain the coating strength. To analyze the coating thickness on a substrate, a cross sectioned specimen was prepared. The coating layer image of the cross-section specimen was obtained using SEM and EDX. The thickness was analyzed through the ImageJ program (Wayne Rasband, NIH).

Structural Analysis of Coating Layer: After coating HAp by LISSC method, a cross section specimen was prepared using a focused ion beam (FIB; Helios NanoLab 600, FEI). The structure of the coating layer was measured by TEM (Talos, FEI), and elemental analysis was performed by high-angle annular dark-field imaging (HAADF).

Analysis of Apatite Forming Principle Using Laser Fixed Spot Irradiation: The effect of laser irradiation on HAp formation was evaluated. To check the effect of the laser irradiation, titanium specimens were immersed in distilled water, DMEM, and MACS, respectively. The laser irradiation conditions were the same as the LISSC method without laser scanning for 15 min with the beam focusing fixed spot. Following laser irradiation, the completed specimen was immersed in distilled water for 10 min and washed repeatedly three times. The washed specimens were dried in a desiccator for at least 12 h, followed by optical microscopy and 3D image measurements.

Surface Roughness Analysis: The surface roughness of titanium (Ti), P10-L50, and P10-L100 were analyzed using a 3D microscope (OLS-5000, Olympus). The values of Ra and Rz were measured using $n = 5$ or more specimens. Graphs show the mean, standard error, and raw values together and statistical significance determined using the Origin program (OriginLab Corporation) statistical analysis tool. Three groups were analyzed by one-way ANOVA with post hoc Tukey's honest significant difference (HSD) test. *, **, *** indicate statistical significant difference when directly compared to each respective group with * $p < 0.05$, ** $p < 0.01$, *** $p < 0.001$.

Contact Angle Analysis: The contact angles of titanium (Ti), P10-L50, and P10-L100 specimens were measured using a contact angle meter (SDS-TEZD, Femtofab) by dropping about 10 μ L of distilled water into the specimen in droplet form. Specimens of $n = 5$ or more were measured and expressed as mean \pm standard deviation. When the contact angle cannot be measured because the surface is hydrophilic and exceeds the device's measurement limit, it is marked as "Not detected (N.D.);" and indicated by a red arrow that the time range of water droplets absorbed by the surface.

Evaluation of Osteoblast Attachment on the HAp-Coated Surface: The mouse osteoblast cells (MC3T3-E1, ATCC) were seeded at 5×10^4 cells on each specimen surface and incubated for 3 h at 37 °C, 5% CO₂, and 95% humidity. Cells that did not attach to the surface were removed by washing three times with PBS. Cells attached to the surface of the specimens were fixed with 4% formaldehyde (4% paraformaldehyde in PBS) for 5 min. Cells were permeated by exposure to 0.1% Triton X-100 in PBS for 5 min and washed three times with PBS. Subsequently, the cells were stained with rhodamine-phalloidin (R415, Invitrogen) and DAPI (LS-J1033, Vectashield), and measured using a fluorescence microscope (Axioscope imager A2M, ZEISS). Four images taken at different locations of each specimen were measured using the ImageJ program (NIH) to determine the number of cells per unit area.

Evaluation of Osteoblast Adhesion in Text and Graphic HAp Patterns: The results were measured by SEM and fluorescence microscopy after culturing osteoblasts in the text form's HAp pattern implemented by LISSC and laser direct writing process method. The mouse osteoblast cell line MC3T3-E1 (ATCC) were seeded at 5×10^4 cells on specimen surface and incubated for 24 h at 37 °C, 5% CO₂, 95% humidity. After incubation time, the cells that did not attach to the surface were removed by washing three times with PBS. Cells attached to the surface of the specimens were fixed with 4% formaldehyde (4% paraformaldehyde in PBS) for 5 min. Cells were permeated by exposure to 0.1% Triton X-100 in PBS for 5 min and washed three times with PBS. F-actin was stained (orange) with rhodamine-phalloidin (R415, Invitrogen), and the nucleus was stained (blue) with DAPI (LS-J1033, Vectashield) and measured using a fluorescence microscope (Axioscope imager A2M, ZEISS).

Analysis of Osteoblast Behavior in the HAp, Non-HAp Interface Implemented by the LISSC Method: The mouse osteoblast cell line MC3T3-E1 (ATCC) was seeded at 5×10^5 cells on specimen surface and incubated for 24 h at 37 °C, 5% CO₂, and 95% humidity. After incubation and staining the cells attached to the HAp and non-HAp interfaces with nucleus (DAPI, LS-J1033, Vectashield) and F-actin (rhodamine-phalloidin, R415, Invitrogen), images were obtained using a fluorescence microscope (Axioscope imager A2M, ZEISS).

Comparison of the Effect of HAp Coating Using LISSC on the Amount of Serum Protein, Fibronectin, and Vitronectin Adsorption: The 10% mouse serum (# 10410, Invitrogen) was placed on the surface of the specimen and maintained at 37 °C for 30 min, followed by washing three times with PBS (PR2004-100-74, Biosesang) to remove non-specifically attached protein. RIPA buffer (# 89900, Thermo) was placed on the specimen surface for 10 min at 4 °C to separate the attached protein from the surface. Protein samples obtained from each surface were measured by the micro-BCA (# 23235, Thermo) and absorbance at 562 nm wavelength using an absorbance meter (GloMax GM3000, Promega). For the analysis of fibronectin and vitronectin adsorption amounts, protein-adsorbed samples were obtained for each specimen using the same method as total serum protein adsorption, as described above. In fluorescence staining of fibronectin, fibronectin antibody (ab2413, abcam) was used as the primary antibody and Alexa Fluor 488 (ab150077, abcam) was used as the secondary antibody. For vitronectin, vitronectin antibody (ab45139, abcam) was used as the primary antibody and Alexa Fluor 594 (ab150080, abcam) was used as the secondary antibody. The fluorescence stained specimens for each protein using antibodies were measured using a fluorescence microscope (Axioscope imager A2M, ZEISS).

Statistical Significance Analysis: All graphs show the mean, standard deviation, and raw values together where $n \geq 4$ and statistical significance determined using the Origin program (Ver9.0, OriginLab Corporation) statistical analysis tool. A two-tailed Student's *t*-test was used when only two groups were being compared. More than three groups were analyzed by one-way ANOVA with post hoc Tukey's honest significant difference (HSD) test. *, **, ***, and **** indicate statistical significant difference when directly compared to each respective group with * $p < 0.05$, ** $p < 0.01$, *** $p < 0.001$, **** $p < 0.0001$.

Supporting Information

Supporting Information is available from the Wiley Online Library or from the author.

Acknowledgements

S.-H.U. and Y.-W.C. contributed equally to this work. This work was supported by the National Research Foundation of Korea (NRF) grant funded by the Korea government (MSIT) (No. 2020R1A2C2010413) and the KIST project (2E30341).

Conflict of Interest

The authors declare no conflict of interest.

Keywords

bioactive coatings, hydroxyapatite hydrothermal syntheses, laser surface treatments

Received: June 21, 2020

Revised: August 5, 2020

Published online: September 15, 2020

- [1] X. Wang, S. Xu, S. Zhou, W. Xu, M. Leary, P. Choong, M. Qian, M. Brandt, Y. M. Xie, *Biomaterials* **2016**, *83*, 127.
- [2] S. Das, K. Dholam, S. Gurav, K. Bendale, A. Ingle, B. Mohanty, P. Chaudhari, J. R. Bellare, *Sci. Rep.* **2019**, *9*, 17638.
- [3] M. Kaur, K. Singh, *Mater. Sci. Eng. C* **2019**, *102*, 844.
- [4] M. Takemoto, S. Fujibayashi, M. Neo, J. Suzuki, T. Kokubo, T. Nakamura, *Biomaterials* **2005**, *26*, 6014.
- [5] S. Nemat-Nasser, W. Guo, J. Cheng, *Acta Mater.* **1999**, *47*, 3705.
- [6] F. Nudelman, P. Pieterse, A. George, P. H. Bomans, H. Friedrich, L. J. Brylka, P. A. Hilbers, G. de With, N. A. Sommerdijk, *Nat. Mater.* **2010**, *9*, 1004.
- [7] O. Geuli, N. Metoki, N. Eliaz, D. Mandler, *Adv. Funct. Mater.* **2016**, *26*, 8003.
- [8] I. Cacciotti, in *Handbook of Bioceramics and Biocomposites*, Springer, New York **2016**, p. 145.
- [9] I. Cacciotti, *Int. J. Appl. Ceram. Technol.* **2019**, *16*, 1864.
- [10] G. Darimont, R. Cloots, E. Heinen, L. Seidel, R. Legrand, *Biomaterials* **2002**, *23*, 2569.
- [11] G. Wang, J. Li, K. Lv, W. Zhang, X. Ding, G. Yang, X. Liu, X. Jiang, *Sci. Rep.* **2016**, *6*, 31769.
- [12] D. V. Vasudev, J. L. Ricci, C. Sabatino, P. Li, J. R. Parsons, *J. Biomed. Mater. Res.* **2004**, *69A*, 629.
- [13] S. C. Leeuwenburgh, J. G. Wolke, M. C. Siebers, J. Schoonman, J. A. Jansen, *Biomaterials* **2006**, *27*, 3368.
- [14] D.-M. Liu, Q. Yang, T. Troczynski, *Biomaterials* **2002**, *23*, 691.
- [15] F. Zhang, S. Cai, G. Xu, F. Wang, N. Yu, R. Ling, X. Wu, *Ceram. Int.* **2016**, *42*, 18466.
- [16] K. Batebi, B. Abbasi Khazaei, A. Afshar, *Surf. Coat. Technol.* **2018**, *352*, 522.
- [17] N. Hijón, M. Victoria Cabañas, J. Peña, M. Vallet-Regí, *Acta Biomater.* **2006**, *2*, 567.
- [18] E. Salahinejad, R. Vahedifard, *Mater. Design* **2017**, *123*, 120.
- [19] M. Manso, C. Jiménez, C. Morant, P. Herrero, J. M. Martiñez-Duart, *Biomaterials* **2000**, *21*, 1755.
- [20] S. Liu, H. Li, L. Zhang, X. Yin, Y. Guo, *Mater. Sci. Eng. C* **2017**, *79*, 100.
- [21] A. Stoch, A. Brozek, G. Kmita, J. Stoch, W. Jastrzębski, A. Rakowska, *J. Mol. Struct.* **2001**, *596*, 191.
- [22] E. Mahlooji, M. Atapour, S. Labbaf, *Carbohydr. Polym.* **2019**, *226*, 115299.
- [23] M. Chambard, O. Marsan, C. Charvillat, D. Grossin, P. Fort, C. Rey, F. Gitzhofer, G. Bertrand, *Surf. Coat. Technol.* **2019**, *371*, 68.
- [24] V. Shamray, V. Sirotkin, I. Smirnov, V. Kalita, A. Y. Fedotov, S. Barinov, V. Komlev, *Ceram. Int.* **2017**, *43*, 9105.
- [25] Y. Yang, K.-H. Kim, J. L. Ong, *Biomaterials* **2005**, *26*, 327.
- [26] S. Thanka Rajan, M. Karthika, A. Bendavid, B. Subramanian, *Appl. Surf. Sci.* **2016**, *369*, 501.
- [27] H. Herø, H. Wie, R. B. Jørgensen, I. E. Ruyter, *J. Biomed. Mater. Res.* **1994**, *28*, 343.
- [28] M. Buchi Suresh, P. Biswas, V. Mahender, R. Johnson, *Mater. Sci. Eng. C* **2017**, *70*, 364.
- [29] M. B. Suresh, P. Biswas, V. Mahender, R. Johnson, *Mater. Sci. Eng. C* **2017**, *70*, 364.
- [30] W.-H. Song, Y.-K. Jun, Y. Han, S.-H. Hong, *Biomaterials* **2004**, *25*, 3341.
- [31] H.-W. Kim, Y.-H. Koh, L.-H. Li, S. Lee, H.-E. Kim, *Biomaterials* **2004**, *25*, 2533.
- [32] E. Mohseni, E. Zalnezhad, A. R. Bushroa, *Int. J. Adhes. Adhes.* **2014**, *48*, 238.
- [33] R. I. M. Asri, W. S. W. Harun, M. A. Hassan, S. A. C. Ghani, Z. Buyong, *J. Mech. Behav. Biomed. Mater.* **2016**, *57*, 95.
- [34] K. Anselme, *Biomaterials* **2000**, *21*, 667.
- [35] C. T. Kwok, P. K. Wong, F. T. Cheng, H. C. Man, *Appl. Surf. Sci.* **2009**, *255*, 6736.
- [36] I. Pereiro, C. Rodríguez-Valencia, C. Serra, E. L. Solla, J. Serra, P. González, *Appl. Surf. Sci.* **2012**, *258*, 9192.
- [37] L. Duta, F. N. Oktar, G. E. Stan, G. Popescu-Pelin, N. Serban, C. Luculescu, I. N. Mihailescu, *Appl. Surf. Sci.* **2013**, *265*, 41.
- [38] H. Nishikawa, T. Hasegawa, A. Miyake, Y. Tashiro, Y. Hashimoto, D. H. A. Blank, G. Rijnders, *Mater. Lett.* **2016**, *165*, 95.
- [39] J. Rau, R. Teghil, M. Fosca, A. De Bonis, I. Cacciotti, A. Bianco, V. R. Albertini, R. Caminiti, A. Ravaglioli, *Mater. Res. Bull.* **2012**, *47*, 1130.
- [40] F. A. Shah, M. L. Johansson, O. Omar, H. Simonsson, A. Palmquist, P. Thomsen, *PLoS One* **2016**, *11*, e0157504.
- [41] C.-S. Chien, T.-Y. Liao, T.-F. Hong, T.-Y. Kuo, C. Chang, M.-L. Yeh, T.-M. Lee, *J. Med. Biol. Eng.* **2014**, *34*, 109.
- [42] J. Yeo, S. Hong, M. Wanit, H. W. Kang, D. Lee, C. P. Grigoropoulos, H. J. Sung, S. H. Ko, *Adv. Funct. Mater.* **2013**, *23*, 3316.
- [43] J. Yeo, S. Hong, W. Manrotkul, Y. D. Suh, J. Lee, J. Kwon, S. H. Ko, *J. Phys. Chem. C* **2014**, *118*, 15448.
- [44] A. Joseph Nathanael, A. Oyane, M. Nakamura, M. Mahanti, K. Koga, K. Shitomi, H. Miyaji, *Acta Biomater.* **2018**, *79*, 148.
- [45] A. Oyane, M. Kakehata, I. Sakamaki, A. Pyatenko, H. Yashiro, A. Ito, K. Torizuka, *Surf. Coat. Technol.* **2016**, *296*, 88.
- [46] A. Oyane, M. Nakamura, I. Sakamaki, Y. Shimizu, S. Miyata, H. Miyaji, *PLoS One* **2018**, *13*, e0206524.
- [47] R. Rohanizadeh, R. Z. LeGeros, M. Harsono, A. Bendavid, *J. Biomed. Mater. Res., Part A* **2005**, *72A*, 428.
- [48] R. B. Heimann, *J. Therm. Spray Technol.* **2016**, *25*, 827.
- [49] W.-L. Yu, T.-W. Sun, C. Qi, H.-K. Zhao, Z.-Y. Ding, Z.-W. Zhang, B.-B. Sun, J. Shen, F. Chen, Y.-J. Zhu, D.-Y. Chen, Y.-H. He, *Sci. Rep.* **2017**, *7*, 44129.
- [50] M. Nakayama, S. Kajiyama, A. Kumamoto, T. Nishimura, Y. Ikuhara, M. Yamato, T. Kato, *Nat. Commun.* **2018**, *9*, 568.
- [51] K. Yamagishi, K. Onuma, T. Suzuki, F. Okada, J. Tagami, M. Otsuki, P. Senawangse, *Nature* **2005**, *433*, 819.
- [52] C. L. A. Leung, S. Marussi, R. C. Atwood, M. Towrie, P. J. Withers, P. D. Lee, *Nat. Commun.* **2018**, *9*, 1355.
- [53] C. Zhao, K. Fezzaa, R. W. Cunningham, H. Wen, F. De Carlo, L. Chen, A. D. Rollett, T. Sun, *Sci. Rep.* **2017**, *7*, 3602.
- [54] W. Meng, Z. Li, F. Lu, Y. Wu, J. Chen, S. Katayama, *J. Mater. Process. Technol.* **2014**, *214*, 1658.
- [55] M. Miyagi, H. Wang, R. Yoshida, Y. Kawahito, H. Kawakami, T. Shoubu, *Sci. Rep.* **2018**, *8*, 12944.
- [56] D. Vogel, H. Dempwolf, A. Baumann, R. Bader, *J. Mech. Behav. Biomed. Mater.* **2018**, *77*, 600.
- [57] J. Cizek, J. Matejicek, *J. Therm. Spray Technol.* **2018**, *27*, 1251.
- [58] T. Roland, H. Pelletier, J. Krier, *J. Appl. Electrochem.* **2013**, *43*, 53.
- [59] R. Asmawi, M. H. I. Ibrahim, A. M. Amin, N. Mustafa, Z. Noranai, *IOP Conf. Ser.: Mater. Sci. Eng.* **2017**, *226*, 012179.
- [60] P. Rajesh, C. Muraleedharan, M. Komath, H. Varma, *J. Mater. Sci.: Mater. Med* **2011**, *22*, 497.
- [61] J. L. Arias, M. B. Mayor, J. Pou, Y. Leng, B. León, M. Pérez-Amor, *Biomaterials* **2003**, *24*, 3403.
- [62] Y. Duan, S. Zhu, F. Guo, J. Zhu, M. Li, J. Ma, Q. Zhu, *Arch. Med. Sci.* **2012**, *2*, 199.
- [63] S. Ban, J. Hasegawa, *Biomaterials* **2002**, *23*, 2965.
- [64] J. T. Y. Lee, Y. Leng, K. L. Chow, F. Ren, X. Ge, K. Wang, X. Lu, *Acta Biomater.* **2011**, *7*, 2615.
- [65] H.-M. Kim, T. Himeno, T. Kokubo, T. Nakamura, *Biomaterials* **2005**, *26*, 4366.
- [66] K. Mori, T. Hara, T. Mizugaki, K. Ebitani, K. Kaneda, *J. Am. Chem. Soc.* **2004**, *126*, 10657.
- [67] S. Sugiyama, Y. Iguchi, H. Nishioka, T. Minami, T. Moriga, H. Hayashi, J. B. Moffat, *J. Catal.* **1998**, *176*, 25.
- [68] L. B. Kong, J. Ma, F. Boey, *J. Mater. Sci.* **2002**, *37*, 1131.
- [69] Y. W. Gu, B. Y. Tay, C. S. Lim, M. S. Yong, *Nanotechnology* **2006**, *17*, 2212.
- [70] P. Siriphannon, Y. Kameshima, A. Yasumori, K. Okada, S. Hayashi, *J. Biomed. Mater. Res.* **2002**, *60*, 175.

- [71] M. Tanahashi, T. Yao, T. Kokubo, M. Minoda, T. Miyamoto, T. Nakamura, T. Yamamuro, *J. Am. Ceram. Soc.* **1994**, *77*, 2805.
- [72] A. C. Tas, S. B. Bhaduri, *J. Mater. Res.* **2004**, *19*, 2742.
- [73] M. B. Rahmany, M. Van Dyke, *Acta Biomater.* **2013**, *9*, 5431.
- [74] P. Roach, D. Farrar, C. C. Perry, *J. Am. Chem. Soc.* **2005**, *127*, 8168.
- [75] N. Huebsch, D. J. Mooney, *Nature* **2009**, *462*, 426.
- [76] J. J. Green, J. H. Elisseeff, *Nature* **2016**, *540*, 386.
- [77] M. C. Siebers, P. J. ter Brugge, X. F. Walboomers, J. A. Jansen, *Biomaterials* **2005**, *26*, 137.
- [78] K. M. Woo, J. Seo, R. Zhang, P. X. Ma, *Biomaterials* **2007**, *28*, 2622.
- [79] A. Shekaran, A. J. García, *J. Biomed. Mater. Res., Part A* **2011**, *96A*, 261.
- [80] M. M. Martino, F. Tortelli, M. Mochizuki, S. Traub, D. Ben-David, G. A. Kuhn, R. Müller, E. Livne, S. A. Eming, J. A. Hubbell, *Sci. Transl. Med.* **2011**, *3*, 100ra89.